



ELSEVIER

Available online at www.sciencedirect.com

SCIENCE @ DIRECT®

Earth and Planetary Science Letters 234 (2005) 15–25

EPSL

www.elsevier.com/locate/epsl

The role of convective mixing in degassing the Earth's mantle

Nicolas Coltice

*Laboratoire de Sciences de la Terre UMR 5570, Université Lyon 1, Bat. Géode, 43 Bd du 11 Novembre 1918,
69622 Villeurbanne CEDEX, France*

Received 7 July 2004; received in revised form 21 February 2005; accepted 24 February 2005

Available online 19 April 2005

Editor: R.D. van der Hilst

Abstract

The chemical evolution of the mantle depends on the way rocks are processed at the surface of the Earth and on the efficiency of convective mixing. In order to quantify how mixing and processing depend on convection parameters (Rayleigh number, heating mode and viscosity stratification), I conducted an extensive set of simple 2D convection simulations with passive tracers and compute (a) bulk Lagrangian strain rates to evaluate mixing efficiency and (b) processing histories. At high Rayleigh number, the strain rate is only a function of the velocity of the flow, whatever the heating mode or viscosity stratification. This is not the case in low Rayleigh number experiments with basal heating where a transition regime is observed with inefficient mixing though chaotic. The simulations show that the processing efficiency depends a lot on the heating mode: the probability of sampling primordial rocks is larger with internal heating than with basal heating. Scaling laws are proposed to parameterize mantle processing histories and it is predicted that in a 300 K hotter Earth, convection can account for the early degassing of the mantle (more than 90% in less than 100 Myr).

© 2005 Elsevier B.V. All rights reserved.

Keywords: mantle convection; geochemistry; mixing; degassing; primitive mantle

1. Introduction

In the search of a holistic view of the chemical evolution of the Earth's mantle, many models have been proposed with the goal of matching geophysical and geochemical observations [1,2]. On one hand geophysical models can explain thermal histories but do not explain fully the complexity of geochemical observations [3–5]. On the other hand, geochemical

models are built to fit the chemical data [6–8] but contradict the physics of the mantle [9,10]. Recently, sophisticated modeling of the chemical evolution of the mantle incorporating plate-like behavior got closer to the achievement of computing accurate and Earth-like thermo-chemical simulations [11]. Though, computing a realistic mantle evolution from first principles involves a complexity beyond our present day capabilities.

The two major links between the physics of convection and the chemistry of mantle rocks are the

E-mail address: coltice@univ-lyon1.fr.

processes of mixing and extraction at mid ocean ridges. Mechanical mixing studies tend to show that because mixing is chaotic, it is doubtful to predict the mixing properties of a flow from simple flow parameters [12–15]. Especially, the deformation of a heterogeneity introduced in a flow depends drastically on details of the velocity field. However, most of these works employ analytic Stokes flows or imposed surface velocities neglecting the role of self-organization of convection, and focus on the spatial mixing pattern instead of average mixing behavior. Hence, the question of a relationship between convection parameters and average mixing efficiency remains.

Processing at mid ocean ridges has been treated mostly in studies of isotopic evolution of the mantle [11,16]. It has been shown that homogeneous convection rapidly processes the whole mantle domain and that isolation of pristine regions is not possible unless models involve intrinsic density and viscosity differences in the medium [2]. Although, quantifications of how convection parameters influence processing still have to be done. Though unsatisfactory [19], box models (where processing decays as a function of the residence time) represent the most common analytic tool to perform chemical evolution simulations [17,18].

The aim of the present paper is to extract quantitative relationships between physical parameters of convection (Rayleigh number, heating mode, viscosity stratifications), mixing and processing through an extensive set of 2D numerical simulations of free homogeneous convection. These calculations are further motivated by two other objectives: building parameterized models more physically sounded than box-models and contributing to constrain the history of mantle degassing.

The numerical setup is first described introducing the primordial variables used to measure mixing and processing. Then the roles of the Rayleigh number, heating mode and viscosity stratification are detailed. Finally, the relevance of the results of the 2D simulations and the consequences of this study for the Earth's mantle are discussed.

2. Experimental setup

To explore relationships between convection, mixing and chemical histories, I propose an

experimental setup based on fluid mechanics, physics of mixing and analytical processing models.

2.1. Fluid mechanics setup

To compute convective flows with uniform physical properties (except the viscosity that varies with depth in some experiments), the Navier–Stokes equations are solved using the well benchmarked finite-element convection code ConMan [20]. I choose a 2:1 Cartesian box for the calculations to allow an extensive exploration of the parameter space. To check that the results do not depend on geometry, I build a smaller set of experiments with a larger box of aspect ratio 8:1. Free slip boundary conditions are applied on the edges of the boxes. In all experiments, the initial conditions correspond to a statistical steady state, which means that there is statistically no cooling in those models (heat sources equal surface heat loss). I have checked that the mixing and processing results presented here do not depend on initial conditions by repeating the experiments with two different initial states when convection is intrinsically time-dependent.

In the simulations, I use different expressions for the Rayleigh number Ra depending on the heating mode of the system. For internal heating, this is

$$Ra_i = \frac{\alpha \rho^2 g H L^5}{k \kappa \mu},$$

where α is the thermal expansivity, ρ the reference density, g the gravitational acceleration, H the rate of internal heating per unit of mass, L the reference height of the system, k the thermal conductivity, κ the thermal diffusivity and μ the dynamic viscosity. With Earth values, Ra_i is close to 10^9 . For basal and partial basal heating

$$Ra_b = \frac{\alpha \rho g \Delta T L^3}{\kappa \mu},$$

is used where ΔT is the temperature difference between the bottom and top boundaries (Ra_b is close to 10^8 for the mantle).

To follow stretching and mimic the chemical evolution of the system, passive particles are tracked

into the flow. Their position x into the convection box evolves according to

$$\frac{\partial x}{\partial t} = u(x,t),$$

u being the local velocity. To solve this equation, a time integration method and an interpolation of the velocity between grid nodes are needed. For sake of consistency, the velocity of a particle lying between grid nodes is naturally interpolated with the bilinear shape functions of the finite element formulation in ConMan [21]. A fifth-order Runge–Kutta scheme is used for the time integration. In the simulations, I have checked that the number of particles is always statistically sufficient (increasing this number does not change the results).

2.2. Mixing setup

Two simple models can describe the two end-members of mixing dynamics: regular (or laminar) and chaotic (or turbulent) mixing [22]. Regular mixing occurs in 2D steady-state flows where the trajectories of particles are identical to streamlines. In this regime, an initial distance l_0 between two particles is stretched into a new distance l that increases linearly with time and proportionally to the strain rate. The stretching of a distance is parameterized by

$$\varepsilon = \frac{l}{l_0},$$

which depends linearly on the time as

$$\varepsilon(t) = 1 + \dot{\varepsilon}t, \tag{1}$$

where $\dot{\varepsilon}$ is the Lagrangian strain rate. The Lagrangian strain rate is the strain rate experienced locally by the line as it is moving into the flow. In the calculations, the Lagrangian strain rate is always lower than the Eulerian strain rate which is the second invariant of the local strain rate tensor.

Chaotic mixing occurs when the dimensionality of the system is larger and where particle trajectories get more complex. In 2D, time-dependent systems show this behavior and two particles can follow completely

different path-lines though they were infinitely close initially. In 3D, even steady flows can produce chaotic Lagrangian mixing, enhanced by the presence of a toroidal component [23]. Stretching in such a flow evolves exponentially with time

$$\varepsilon(t) = \exp(\dot{\varepsilon}t).$$

The simplicity of these models is that they only depend on one parameter, the Lagrangian strain rate $\dot{\varepsilon}$. This parameter is chosen to be the quantitative measurement of average mixing in the numerical experiments. As illustrated by Fig. 1, the numerical experiments display strain evolutions that can be well explained by one of the two end-members of mixing dynamics.

To compute the local stretching ε around a particle, I follow the distance between two initially very close particles. The larger the distance, the larger the error on the local stretching. Hence, this distance has to be renormalized along the direction of stretching at every time step [23]. At a time t , the estimate of the Lagrangian strain rate is

$$\dot{\varepsilon} = \frac{\log(\varepsilon)}{t}.$$

The bulk Lagrangian strain rate is the average over all the couples of particles (20,000 were sufficient). In regular mixing flows, the computed $\dot{\varepsilon}$ would be much lower than the theoretical $\dot{\varepsilon}$ of Eq. (1).

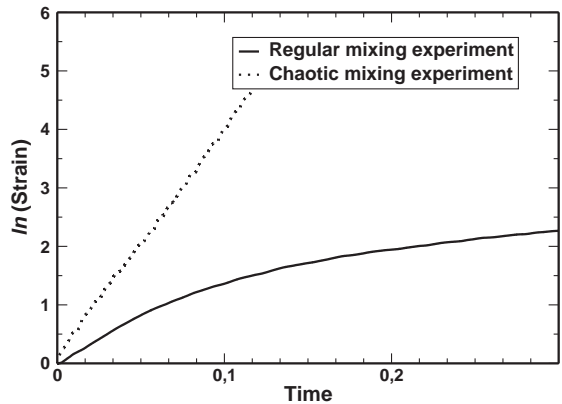


Fig. 1. Strain as a function of time in two convection simulations illustrating regular mixing (internal heating, $Ra_i=10^6$) and chaotic mixing (basal heating, $Ra_b=10^5$).



Fig. 2. Examples of model setup (small and large box) with the black solid line being the depth of sampling. The grayscale represents the temperature fields in basally heated simulations at $Ra_b=10^7$ and viscosity jump of 100.

2.3. Processing setup

Processing of mantle rocks occurs when they melt at shallow depth. For modeling the processing, there is no need to use realistic melting models because explicitly computing melt formation and removal is time consuming and simply out of reach (building a physical theory is still a challenge [24]). In the aim of exploring the parameter space, another method is chosen though simplistic. First, pristine rocks are modeled by particles advected in the flow that are removed once they melt. In the Earth, almost each rock that reaches the surface is partially melted. Hence, I choose a melting depth above which every particle is removed to simulate subsurface melting and extraction. This depth is 150 km for every experiment (see Fig. 2). Increasing this value by a factor of 2 decreases the computed time scales by about a factor of 2 as well.

Somewhat in parallel with mixing, two extreme regimes can be expected for the processing of rocks in a convective system. The first is linear processing, where

the evolution of the extracted fraction E (varying between 0 and 100%) with times follows

$$E(t) = \frac{t}{t_p}, \quad E(t) \leq E_m \quad (2)$$

where t_p is the time it would take to completely process the whole volume. E_m is the maximum fraction that can be processed in the model. Taking a constant mass flux processed at ridges of 10^{15} kg yr^{-1} , the mantle would be completely degassed after 4 billion years. Linear processing states that the sampled material has always the same composition. It implicitly assumes that recycled material is never sampled again until t_p after which only recycled material would be processed.

Another regime would correspond to random sampling [12]:

$$E(t) = E_m \left(1 - \exp \left[-\frac{t}{t_p} \right] \right) \quad (3)$$

where t_p is the processing time of the system. This model implicitly states that the processed fraction at

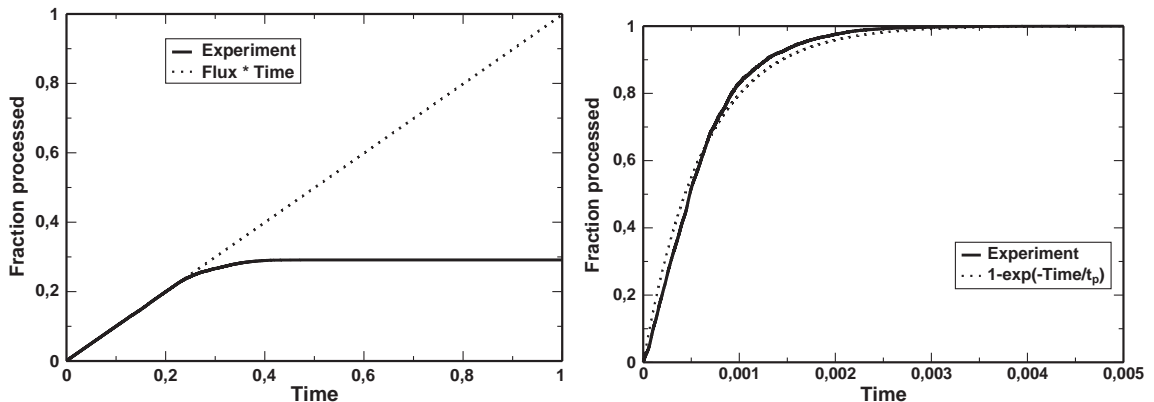


Fig. 3. Examples of numerical experiments of processing showing on the left linear processing (internal heating, $Ra_i=10^4$) and on the right random sampling (internal heating, $Ra_i=10^{10}$).

time t is proportional to the fraction of pristine particles in the box. In other words, the random sampling model assumes the existence of convective mixing.

One can notice that a geochemical box model is a singular random sampling model where t_p exactly equals the mass residence time t_r

$$t_r = E_m/F,$$

where F is the mass flux processed (monitored in the following numerical experiments). The box model states that the composition of rocks being sampled is the same as the mean composition of the whole volume.

To compute t_p and E_m , particles are advected in the flow as long as they reach the sampling depth where $E(t)$ is incremented. $E(t)$ is then fitted to the simple analytic models Eqs. (2) and (3) using a least-squared method. This simple inversion provides the parameters t_p and E_m . In most 2:1 simulations, I use 250,000 particles. The fit quality of the results of the numerical simulations is shown in Fig. 3 and correlation coefficients higher than 0.95 are always found.

It is already an interesting result in itself to demonstrate that the complex system of coupled equations of convection with chemical evolution has a simple solution $E(t)$ that can be parameterized. Indeed, the analytical expression of box models captures the physics of the convection simulations though t_p may not be t_r . So t_p and E_m are parameters of choice to quantify processing in the simulations.

3. Mixing, heating mode and viscosity stratification

In this section, the numerical experiments show that there is a relationship between $\dot{\epsilon}$ and Ra , that mixing in internally heated convection differs from that of basally heated convection, and the viscosity stratification does not impede mixing.

3.1. Heating mode

Fig. 4a and b depict the strain rate as a function of the Rayleigh number for basal and internal heating, respectively. The main observation is that

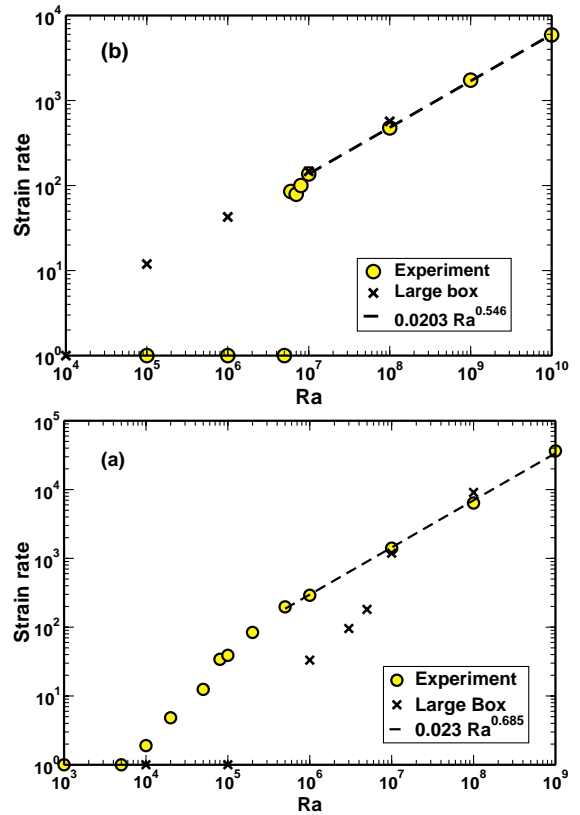


Fig. 4. Lagrangian strain rate as a function of Ra in (a) basally heated experiments and (b) internally heated experiments. The lowest strain rates correspond to laminar mixing. At high Ra , scaling laws fit the experiments.

at sufficiently high Rayleigh number (4×10^5 for basal heating and 5×10^6 for internal heating in the small box), a scaling law exists between Ra and $\dot{\epsilon}$. The Lagrangian strain rate is proportional to $Ra_b^{2/3}$ with bottom heating, and $Ra_i^{1/2}$ with internal heating. These scalings have exponents similar to those for the velocity. It means that with increasing Ra , mixing becomes more efficient only because flow velocities are higher and not because the flow pattern gets more time-dependent. The Lagrangian strain rate is only a function of the velocity of the flow at high Rayleigh number.

At lower Rayleigh number, a significant difference between basal and internal heating is observed. As seen in Fig. 4b where heating is purely internal, mixing is regular as long as Ra_i is lower than a threshold above which mixing becomes chaotic and scales with the velocity. The threshold is exactly at

5×10^6 in the small box and 10^5 in the large box. For basally heated convection (Fig. 4a), laminar mixing occurs for Ra_b close to critical (~ 1000), followed by an intermediate state where mixing is chaotic and $\dot{\epsilon}$ scales with $Ra_b^{1.29}$ (between $Ra_b = 10^4$ and 4×10^5 in the small box and between 10^5 and 10^7 in the large box) until it reaches the $Ra_b^{2/3}$ branch already described.

In 2D, the jump from regular to chaotic mixing occurs when thermal convection becomes time-dependent [22,13]. The intermediate mixing rates observed for basal heating correspond to a transition regime with mostly oscillatory flows. In the oscillatory regime, downwellings and upwellings oscillate but no new instability appears. In other words, inter-cell mixing does not exist. In fully time-dependent flow, new instabilities constantly appear which is the driving mechanism for inter-cell mixing [25]. In internally heated convection, there is no transition between the steady and unsteady regime leading to a sharp threshold between regular and chaotic mixing.

In Fig. 4a, the large box calculations need a higher Ra_b to reach the fully chaotic mixing trend. This is the contrary in Fig. 4b that corresponds to internal heating. Since time-dependence is the condition for chaotic mixing, these results indicate that the long wavelengths of the flow favor unsteadiness with internal heating whereas they enhance steadiness with basal heating.

3.2. Viscosity stratification

An increase of viscosity inside the mantle is needed to explain the long wave-length geoid anomalies and plate velocities [26,27]. This discovery was the subject of speculations concerning the efficiency of mixing in the highly viscous lower mantle and some assigned the high viscosity region to a peculiar geochemical domain [28,29]. In the last decade, many convection simulations showed that an increase of viscosity with depth does not impede the flow nor reduces mixing efficiency. Moreover, the shear flow above the viscosity jump enhances stretching [30,15].

The same conclusions can be reached with the results presented in Fig. 5, where viscosity jumps of 100 and 1000 at mid-depth are introduced in the

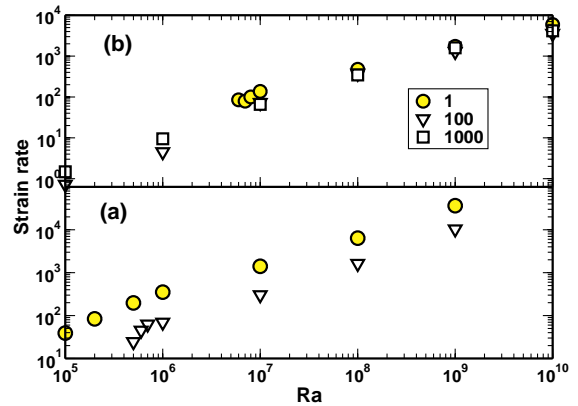


Fig. 5. Lagrangian strain rate as a function of Ra for (a) basally heated and (b) internally heated simulations with viscosity jumps of 100 and 1000. The internally heated cases show no influence of the viscosity stratification.

models. In this figure, Ra corresponds to the Rayleigh number computed with the viscosity of the upper layer and the viscosity jump is the ratio of the higher viscosity over the reference viscosity.

In Fig. 5a corresponding to basal heating, the Lagrangian strain rates obtained with a viscosity jump scale again with the velocity, but are lower than in isoviscous cases with the chosen definition of Ra_b . The same plot shows that the chaotic mixing trend is reached at higher Ra_b than without viscosity stratification. The hot boundary layer is located in the highly viscous region and hence influences the stability and steadiness of starting plumes. For this reason, mixing and the average flow velocities are dependent on Ra and the value of the viscosity jump. Though, the efficiency of mixing still depends on flow velocities only.

In Fig. 5b corresponding to internal heating, mixing is chaotic with a viscosity jump, even at extremely low Ra_i , and the Lagrangian strain rate scales with the velocity. At the same time, the values of strain rates do not depend on the viscosity jump. In fact, the thermal instabilities that drive the flow only depart from the upper low viscosity layer contrarily to the basal heating cases. It appears that the mixing efficiency is only a function of Ra and not of the viscosity stratification with internal heating where the effect of low velocities in the highly viscous region is compensated by strong boundary layer instability.

4. Processing, heating mode and viscosity stratification

Numerical experiments show that heating mode greatly influences processing contrarily to viscosity stratification. In the numerical experiments where mixing is regular, linear processing is observed with E_m close to 0.25. In steady flows, only the streamlines crossing the processing boundary can provide particles, the rest leaving unsampled. In this section, I discuss cases corresponding to random sampling only. They correspond to simulations involving chaotic mixing. The maximum processed fraction is always 100% except in very few viscously stratified experiments (discussed hereafter). In some cases, more than 800 overturns are needed to extract every single particle from the flow.

As discussed above, the mass residence time t_r that would be used in box models is taken for reference and is computed measuring the mass flux across the processing depth. As expected, the flux scales as the velocity for both basal and internal heating modes. As a consequence, t_r scales as $Ra_b^{-2/3}$ with basal heating and as $Ra_i^{-1/2}$ with internal heating. The simulations show that processing is by far more efficient with internal heating and is not influenced by a viscosity stratification.

4.1. Heating from below

Fig. 6a depicts the relationship between the ratio of the processing time t_p over the residence time t_r as a function of Ra_b . A ratio larger than 1 means that the processed material mostly consists in already processed particles. A ratio lower than 1 corresponds to a sampling of material dominated by pristine particles. If the ratio is 1, the sampled material has a concentration of pristine particles identical to that of the whole box.

At high Ra_b , t_p/t_r tends to 1, but for low Ra_b , this ratio can be up to 20. These observations are confirmed in the large box and viscously stratified experiments. These high t_p/t_r mean that already sampled particles have a high probability of being sampled again which occurs when mixing between pristine and sampled regions is poor. Indeed, the simulations with high t_p/t_r correspond to those in the mixing transition branch where $\dot{\epsilon}$ does not scale with the velocity (see Fig. 4a). Inefficient chaotic mixing leads to inefficient process-

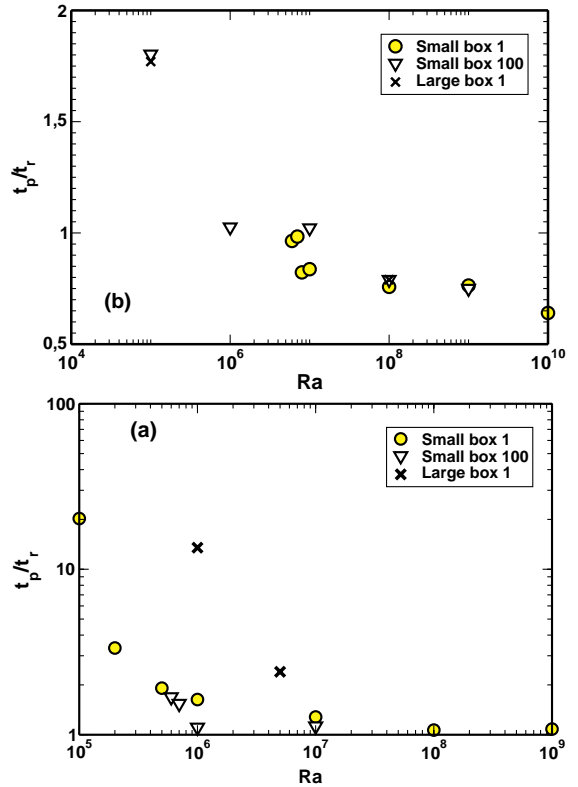


Fig. 6. Processing time as a function of Ra for (a) basally heated experiments and (b) internally heated experiments. Isoviscous and viscosity jumps of 100 are considered. In basally heated cases, the processing time tends towards the residence time whereas it is lower with internal heating.

ing. For these experiments, the box model would overestimate the processing and would not be appropriate. One can notice that t_p is always more than 10% higher than t_r even at higher Ra_b .

The viscosity jump does not play a major role in processing and no major difference is observed in Fig. 6a between isoviscous and viscously stratified cases. However, a slight change exists at low Ra_b concerning the maximum fraction processed. Indeed, E_m is not always 100% with a viscosity jump but consistently closer to 95%. Particles trapped in rolls (similar to corner flow cells) above the viscosity boundary near very stable upwellings or downwellings. These features are enhanced with a constraining geometry but disrupt rapidly in the large box and moderately high Ra_b . Adding 20% of internal heating is also enough to erase these pristine surviving islands.

I have not observed any simple relationship between t_p and $\dot{\epsilon}$. The only implicit relationship between the two variables can be proposed at high Ra_b (where t_p tends towards t_r):

$$t_p \sim t_r = bRa_b^{-2/3} = \frac{a}{\dot{\epsilon}}, \quad (4)$$

a and b being constants depending on the geometry and the setup of the experiment.

4.2. Heating from within

Internally heated convection is again much different as seen in Fig. 6b. When mixing is chaotic, as Ra_i increases t_p becomes lower and lower than t_r , the lowest ratio in the calculations is 0.65. In other words, sampling targets the pristine regions with a higher probability rather than already processed regions. The explanation is that a pristine domain in the core of the flow slowly heats up, becomes buoyant and must rise to the surface to loose its heat. Hence, in internally heated convection, processing would be faster than predicted by a box model at high Ra_i . Numerical experiments conducted with heating from within and from below shows that above 20% of internal heating, processing becomes almost insensitive to the effects of basal heating.

The relationship between mixing efficiency (measured by $\dot{\epsilon}$) and processing efficiency (measured by t_p) is displayed in Fig. 7. When $\dot{\epsilon}$ increases, t_p decreases.

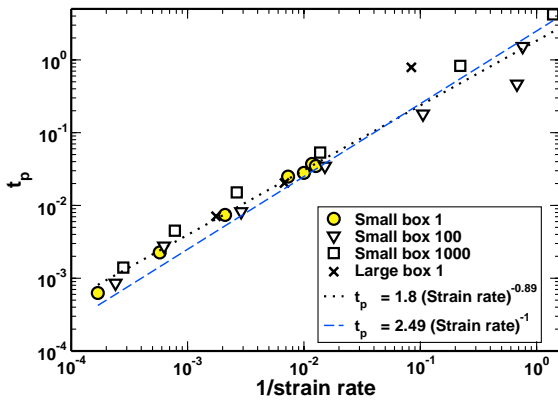


Fig. 7. Processing time as a function of the Lagrangian strain rate for the internally heated simulations (isoviscous and viscously stratified). A least squared fit gives a scaling law where $t_p \propto \dot{\epsilon}^{-0.89}$. A linear fit ($t_p \propto \dot{\epsilon}^{-1}$) is plotted to show that the non-linear scaling law is relevant.

A least squared fit of the couples $(\dot{\epsilon}, t_p)$ gives the following non-dimensional scaling law:

$$t_p \sim 1.8\dot{\epsilon}^{-0.89}. \quad (5)$$

This relationship is almost inverse and one could question the consistency of the difference between the 0.89 exponent and 1, especially at low t_p . Though, Fig. 6b shows a systematic decrease of t_p/t_r with Ra_i which suggests that an exponent lower than 1 in Eq. (5) seems correct.

A surprising observation is that this scaling law holds for isoviscous, viscously stratified, small and large box experiments. It does not seem to depend on the geometry nor the viscosity structure. Hence, knowing the average Lagrangian strain rate in a 2D convection experiment can be used to predict the processing history.

5. Geodynamic interpretations

The simulations provide scaling laws that can be used to parameterize the processing and degassing history of the Earth's mantle.

5.1. Earth's present-day processing rate

From the previous section, I propose two distinctive processing–mixing relationships: (a) mixing and processing efficiency scales as the velocity (the processing time is similar to the mass residence time), (b) mixing efficiency scales with the velocity but processing efficiency scales with mixing efficiency with a 0.9 exponent. Eq. (4) provides the upper bound of the processing time while Eq. (5) the lower bound.

To estimate the present-day processing time, it is necessary to compute the mass residence time which corresponds to the flux of rocks taking part in mid ocean ridge melting. Choosing a plate velocity of 5 cm yr⁻¹, ridge length of 60,000 km and a plate thickness of 150 km leads to an estimate of the residence time of 2.9 Gyr, which is the upper bound of the present day processing time.

The Lagrangian strain rate is needed in Eq. (5) but an accurate estimate for the mantle is desperately hopeless. Though, rough estimates can be proposed from strain rates measured at the surface which range

Table 1
Parameters chosen to compute the temperature dependence of the processing time

| Parameter | Reference value |
|-----------------------|--|
| T_0 | 1600 K |
| L | 2900 km |
| κ | $10^{-6} \text{ m}^2 \text{ s}^{-1}$ |
| E | 500 kJ mol $^{-1}$ |
| $\dot{\epsilon}(T_0)$ | 10^{-16} – 10^{-15} s^{-1} |

between 10^{-16} to 10^{-15} s^{-1} . To use the dimensionless scaling laws, the time has to be scaled by the diffusion time L^2/κ . Hence, the present day processing rates from Eq. (5) range from 0.14 Gyr to 1.13 Gyr, corresponding to lower bonds.

The highest processing time predicts that 6% of the mantle would remain unprocessed today, and the lowest processing time implies that the unprocessed fraction is completely negligible. Since a detectable amount of primordial ^3He is degassed at ridges, either a strain rate of 10^{-15} s^{-1} too large for the mantle or transfers of ^3He within mantle reservoirs have to be invoked [32].

5.2. Early degassing

The goal of scaling laws is to make predictions, and here for a younger Earth. Petrologic and geochemical studies have shown that the Earth’s mantle may have been 200–300 K hotter in the Archaean and maybe more early on [33]. Because the processing rate is related to the mixing rate and Ra , it must have been drastically shorter in the past. To investigate the effect of higher temperature in the Archaean on the processing time, Eqs. (4) and (5) are expressed as a function of the adiabatic temperature T , the present-day adiabatic temperature T_0 , the present-day strain rate $\dot{\epsilon}(T_0)$ in the same way as in thermal history calculations [34,35]:

$$t_p(T) = bRa^{-2/3} = t_p(T_0) \left[\frac{T}{T_0} \right]^{-2/3} \left[\frac{\mu(T_0)}{\mu(T)} \right]^{-2/3}, \quad (6)$$

$$t_p(T) = 1.8 \frac{L^2}{\kappa} \left\{ \dot{\epsilon}(T_0) \frac{L^2}{\kappa} \left[\frac{T}{T_0} \right]^{2/3} \left[\frac{\mu(T_0)}{\mu(T)} \right]^{2/3} \right\}^{-0.89}. \quad (7)$$

Eq. (6) provides the upper bound for $t_p(T)$ and Eq. (7) the lower bound as seen in the previous section. The viscosity of mantle rocks is dependent on the temperature as

$$\mu(T) = \mu_0 \exp\left(\frac{E}{RT}\right) \quad (8)$$

where μ_0 is a reference viscosity and E the activation energy.

The parameters I choose to solve Eqs. (6) and (7) using Eq. (8), are listed in Table 1. For instance, a 300 K hotter mantle would have a viscosity 550 times lower than it is now. The corresponding strain rates are 10^{-14} – 10^{-13} s^{-1} and it would take between 5 and 50 Myr to reduce a heterogeneity from a kilometer-thick to a tenth of millimeter that would be erased by solid-state diffusion.

Fig. 8 depicts the range of processing times as a function of the adiabatic temperature T . In a 300 K hotter mantle, the processing time is between 3 and 50 Myr. These numbers lead to predict that between 87% and ~100% of the mantle would be processed in 100 Myr.

This conclusion agrees with geochemical analysis of short-lived noble gases (like Xe) that showed that the atmosphere was mostly degassed from the mantle very early in the Earth’s history [36]. In some models, 99.9% of the mantle gases are outgassed from the mantle in less than 100 Myr [37].

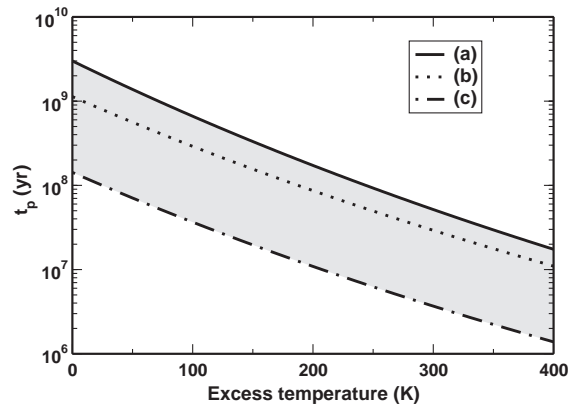


Fig. 8. Processing time as a function of the mantle excess temperature relative to the present-day temperature of 1600 K. (a) Corresponds to the mass residence time equation, (b) to Eq. (5) with a present day reference of $\dot{\epsilon}$ of 10^{-16} s^{-1} and (c) with a present day reference $\dot{\epsilon}$ of 10^{-15} s^{-1} .

6. Conclusions

In the present study, I show that bulk mixing and processing in the mantle can be constrained by the parameters of convection. At high Ra , mixing is chaotic and the mean Lagrangian strain rate scales with the velocity. The heating mode plays a fundamental role in the mixing behavior:

- (a) mixing is inefficient at low Ra ($\dot{\epsilon} \propto Ra^{1.3}$) with bottom heating,
- (b) mixing efficiency does not depend on the viscosity stratification and is only a function of the velocity of the flow,
- (c) mixing is always efficient with internal heating as long as mixing is chaotic, even with a drastic viscosity jump.

Processing in free convection is exponential (fitting a random sampling model) when mixing is chaotic and also depends on heating mode:

- (a) the processing time tends to the mass residence time (box model) at high Ra with bottom heating but is much higher when mixing is not efficient ($\dot{\epsilon} \propto Ra^{1.3}$),
- (b) the processing time is significantly lower than the mass residence time with internal heating.

Hence, scaling laws between processing time, Lagrangian strain rates and Ra can be derived to parameterize the chemical evolution of the mantle. In a 300 K hotter Earth, the catastrophic degassing observed by short-half life radioactive systems like I/ Xe could be explained simply by degassing a convective system like it does today.

The limitations of this study are the introduction of a constant sampling depth and the 2D geometry. As explained above, the sampling depth is an artificial way of simulating melting and does not account for evolution in time of the temperature in the mantle discussed in the last section. It is well known that mixing can be different (and less efficient) in 3D [31,23] and the results presented here could be questioned. But this paper demonstrates that bulk mixing and processing can be parameterized by convection parameters and this should still be valid in 3D since the Rayleigh number is independent of the

geometry. Moreover, including the physics of melting in a 3D convection system is a fundamental achievement to model the chemical evolution of the mantle.

Acknowledgements

I would like to thank Yanick Ricard and Marc Monnereau for their comments and their support. Constructive comments from an anonymous reviewer helped improve the manuscript. This paper benefited from the editorship of Rob van der Hilst. This work was sponsored by the DyETI program of CNRS-INSU.

References

- [1] A.W. Hofmann, Mantle geochemistry: the message from oceanic volcanism, *Nature* 385 (1997) 219–229.
- [2] P.J. Tackley, Mantle convection and plate tectonics: towards an integrated physical and chemical theory, *Science* 288 (2000) 2002–2007.
- [3] L.H. Kellogg, B.H. Hager, R.D. van der Hilst, Compositional stratification in the deep mantle, *Science* 283 (1999) 1881–1884.
- [4] N. Coltice, Y. Ricard, Geochemical observations and one layer mantle convection, *Earth Planet. Sci. Lett.* 174 (1999) 125–137.
- [5] D. Bercovici, S.-I. Karato, Whole mantle convection and the transition-zone water filter, *Nature* 425 (2003) 39–44.
- [6] D. DePaolo, G.I. Wasserburg, Inferences about magma sources and mantle structure from variations of $^{143}\text{Nd}/^{144}\text{Nd}$, *Geophys. Res. Lett.* 3 (1976) 743–746.
- [7] C.J. Allègre, A.W. Hofmann, R.K. O’Nions, The Argon constraints on mantle structure, *Geophys. Res. Lett.* 23 (1996) 3555–3557.
- [8] D. Porcelli, G.J. Wasserburg, Mass transfer of helium, neon, argon and xenon through a steady-state upper mantle, *Geochim. Cosmochim. Acta* 59 (1995) 4921–4937.
- [9] S.P. Grand, R.D. van der Hilst, S. Widiyantoro, Global seismic tomography: a snapshot of convection in the Earth, *GSA Today* 7 (1997) 1–7.
- [10] R. Montelli, G. Nolet, F.A. Dahlen, G. Masters, R.E. Engdahl, S.-H. Hung, Finite-frequency tomography reveals a variety of plumes in the mantle, *Science* 303 (2004) 338–343.
- [11] P.J. Tackley, S. Xie, The thermo-chemical structure and evolution of Earth’s mantle: constraints and numerical models, *Philos. Trans. R. Soc. Lond., A* 360 (2002) 2593–2609.
- [12] M. Gurnis, G.F. Davies, Mixing in numerical models of mantle convection incorporating plate kinematics, *J. Geophys. Res.* 91 (1986) 6375–6395.
- [13] U.R. Christensen, Mixing by time-dependent convection, *Earth Planet. Sci. Lett.* 95 (1989) 382–394.
- [14] G.F. Davies, Comment on “mixing by time-dependent convection”, by U. Christensen, *Earth Planet. Sci. Lett.* 98 (1990) 405–407.

- [15] D.L. Hunt, L.H. Kellogg, Mixing and development of heterogeneities in the mantle: the role of depth-dependent viscosity, *J. Geophys. Res.* 106 (2001) 6747–6759.
- [16] P.E. van Keken, C.J. Ballentine, Dynamical models of mantle volatile evolution and the role of phase transitions and temperature-dependent rheology, *J. Geophys. Res.* 104 (1999) 7137–7168.
- [17] S.B. Jacobsen, G.J. Wasserburg, The mean age of mantle and crustal reservoirs, *J. Geophys. Res.* 84 (1979) 7411–7427.
- [18] F. Albarède, Radiogenic ingrowth in systems with multiple reservoirs: applications to the differentiation of the mantle-crust system, *Earth Planet. Sci. Lett.* 188 (2001) 59–73.
- [19] N. Coltice, S. Ferrachat, Y. Ricard, Box modeling the chemical evolution of geophysical systems: case study of the Earth's mantle, *Geophys. Res. Lett.* 27 (2000) 1579–1582.
- [20] S.D. King, A. Raefsky, B. Hager, ConMan: vectorizing a finite element code for incompressible two-dimensional convection in the Earth's mantle, *Phys. Earth Planet. Inter.* 59 (1990) 196–208.
- [21] O.C. Zienkiewicz, R.L. Taylor, *The Finite Element Method*, 3rd edition, McGraw-Hill, New York, 1977.
- [22] P. Olson, D.A. Yuen, D. Balsiger, Mixing of passive heterogeneities by mantle convection, *J. Geophys. Res.* 89 (1984) 425–436.
- [23] S. Ferrachat, Y. Ricard, Regular vs. chaotic mixing, *Earth Planet. Sci. Lett.* 155 (1998) 75–86.
- [24] D. Bercovici, Y. Ricard, G. Schubert, A two-phase model for compaction and damage: 1. General theory, *J. Geophys. Res.* 106 (2001) 8887–8906.
- [25] J. Schmalzl, U. Hansen, Mixing the Earth's mantle by thermal-convection: a scale dependent phenomenon, *Geophys. Res. Lett.* 21 (1994) 987–990.
- [26] M.A. Richards, B.H. Hager, Geoid anomalies in a dynamic Earth, *J. Geophys. Res.* 89 (1984) 5987–6002.
- [27] Y. Ricard, M.A. Richards, C. Lithgow-Bertelloni, Y. LeStunff, A geodynamic model of mantle density heterogeneity, *J. Geophys. Res.* 98 (1993) 21895–21909.
- [28] G.F. Davies, Geophysical and isotopic constraints on mantle convection: an interim synthesis, *J. Geophys. Res.* 89 (1984) 6017–6040.
- [29] C.J. Allègre, E. Lewin, Isotopic systems and stirring times of the Earth's mantle, *Earth Planet. Sci. Lett.* 136 (1995) 629–646.
- [30] S. Ferrachat, Y. Ricard, Mixing properties in the Earth's mantle: effects of the viscosity stratification and of oceanic crust segregation, *Geochem. Geophys. Geosyst.* 2 (2001).
- [31] J. Schmalzl, G.A. Houseman, U. Hansen, Mixing properties of three-dimensional stationary convection, *Phys. Fluids* 7 (1995) 1027–1033.
- [32] R.K. O'Nions, E.R. Oxburgh, Heat and helium in the Earth, *Nature* 306 (1983) 429–431.
- [33] E.G. Nisbet, M.J. Chedale, N.T. Arndt, M.J. Bickle, Constraining the potential temperature of the Archaean mantle: a review of the evidence from komatiites, *Lithos* 30 (1993) 291–307.
- [34] G.F. Davies, Thermal histories of convective Earth models and constraints on radiogenic heat production in the Earth, *J. Geophys. Res.* 85 (1980) 2517–2530.
- [35] U.R. Christensen, Thermal evolution models for the Earth, *J. Geophys. Res.* 90 (1985) 2995–3007.
- [36] T. Staudacher, C.J. Allègre, Terrestrial xenology, *Earth Planet. Sci. Lett.* 60 (1982) 389–406.
- [37] C.J. Allègre, T. Staudacher, P. Sarda, Rare gas systematics: formation of the atmosphere, evolution and structure of the mantle, *Earth Planet. Sci. Lett.* 81 (1986) 127–150.